The CDF-II Time-of-Flight Detector System

S. Cabrera[a], J. Fernandez[a], G. Gomez[a], J. Piedra[a], T. Rodrigo[a], A. Ruiz[a], I. Vila[a], R. Vilar[a], C. Grozis[b], R. Kephart[b], R. Stanek[b], D.H. Kim[c], M.S. Kim[c], Y. Oh[c], Y.K. Kim[d], G. Veramendi[d], K. Anikeev[e], G. Bauer[e], I.K. Furic[e], A. Korn[e], I. Kravchenko[e], M. Mulhearn[e], C. Paus[e], S. Pavlon[e], K. Sumorok[e], C. Chen[f], M. Jones[f], W. Kononenko[f], J. Kroll[f], G. M. Mayers[f], F. M. Newcomer[f], R. G. C. Oldeman[f], D. Usynin[f], R. Van Berg[f], G. Bellettini[g], C. Cerri[g], A. Menzione[g], F. Spinella[g], E. Vataga[g], S. De Cecco[h], D. De Pedis[h], C. Dionisi[h], S. Giagu[h], M. Rescigno[h], L. Zanello[h], M. Ahn[i], B.J. Kim[i], S.B. Kim[i], I. Cho[j], J. Lee[j], I. Yu[j], H. Kaneko[k], A. Kazama[k], S. Kim[k], K. Sato[k], K. Sato[k], F. Ukegawa[k]

Abstract— **A Time-of-Flight detector (TOF) has been added to the CDF-II experiment to provide charged kaon identification primarily for neutral B meson flavor determination. With its expected 100 ps time-of-flight resolution, the TOF system will be able to provide at least two standard deviation separation between $K^{\pm}$ and $\pi^{\pm}$ for momenta $p < 1.6$ GeV/c, complementing the specific ionization energy loss, dE/dx, measured in the new drift chamber. This paper describes the TOF detector and reports on the initial performance based on the data collected by the CDF-II so far.**

Keywords— **Time-of-Flight, CDF, Particle Identification, Photomultiplier, Scintillator.**

I. Introduction

After a successful Run-I data taking period at the Fermilab Tevatron from 1992 to 1996, the CDF detector detector underwent a major upgrade [1] for Run-II of the Tevatron, which began in March 2001. Based on several years of R&D, including a test system installed in CDF at the end of Run-I, approval was granted for the inclusion of a Time-of-Flight (TOF) detector in the CDF upgrade. The installation of the TOF detector was completed in August 2001 and its data has been included in the CDF-II readout since that time.

During Run-I, particle identification in CDF was based on the specific ionization energy loss, dE/dx, measured in the central drift chamber. The dE/dx measurement provided one standard deviation separation between charged kaons and charged pions for momenta greater than 2 GeV/c. The CDF-II drift chamber, the Central Outer Tracker (COT), maintains this dE/dx performance. The primary physics motivation for TOF is to enhance the particle identification capability to improve neutral B meson flavor determination at production. With an expected time-of-flight resolution of 100 ps, the TOF system will provide at least two standard deviation separation between $K^{\pm}$ and $\pi^{\pm}$ for momenta $p < 1.6$ GeV/c, complementing the dE/dx measurement from the COT.

[a]Instituto de Fisica de Cantabria (Spain)
[b]Fermi National Accelerator Laboratory (USA)
[c]Kyungpook National University (Korea)
[d]Lawrence Berkeley National Laboratory (USA)
[e]Massachusetts Institute of Technology (USA)
[f]University of Pennsylvania (USA)
[g]INFN, University of Pisa (Italy)
[h]INFN, University of Roma (Italy)
[i]Seoul National University (Korea)
[j]SungKyunKwan University (Korea)
[k]University of Tsukuba (Japan)

II. Particle Identification with TOF

Particle identification with TOF is performed by measuring the time of arrival of a particle at the scintillator with respect to the collision time, t_0. The particle mass m can then be determined from the momentum p, the path-length L, and the time-of-flight t:

$$m = \frac{p}{c}\sqrt{\frac{c^2t^2}{L^2} - 1}, \qquad (1)$$

where p and L are measured by the tracking system. Figure 1 shows the time-of-flight difference between K/π, p/K and p/π. For comparison, the separation provided by dE/dx is also shown. The TOF improves substantially the K/π separation in the momentum region $p \leq 1.6$ GeV/c.

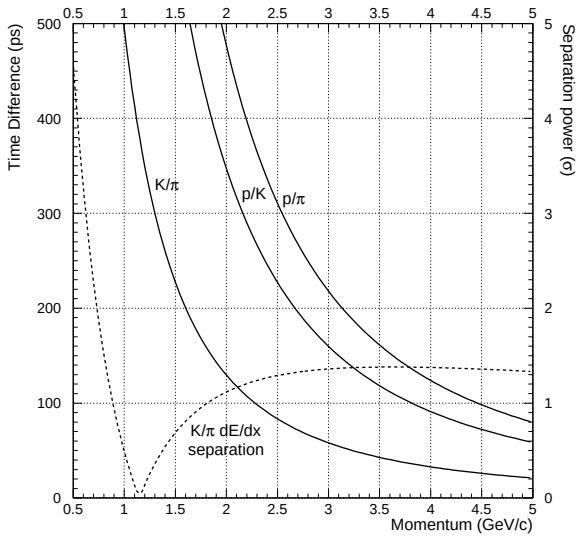

Fig. 1. Time difference as a function of momentum between K/π, p/K and p/π traversing a distance of 140 cm, expressed in ps and separation power, assuming a resolution of 100 ps. The dashed line shows the K/π separation power from the dE/dx measurement in the Central Outer Tracker.

III. The Detector Description

A. Mechanical Design and Photomultiplier Tubes

The CDF Time-of-Flight detector[2][3] consists of 216 bars of $4 \times 4 \times 279\,\text{cm}$ Bicron BC-408 scintillator located at a radius of 138 cm from the beam line in 4.7 cm of radial space between the Central Outer Tracker (COT) and the cryostat for the super-conducting solenoid. The pseudo-rapidity coverage of the system is roughly $|\eta| < 1$. The material thickness of the outer wall of the tracking detector is approximately 10% of a radiation length.

The bars of scintillator were wrapped first in white Tyvek and a layer of black Marvelguard. The bars were assembled in groups of three by interleaving them with thin metal strips attached via springs to the aluminum PMT housing at the ends. The entire assembly was then wrapped again in black Kevlar. The scintillator assemblies at the top of the detector do not have any of their weight supported by the COT, as this could deflect the COT end-plates. Instead, the scintillator assembles located at ϕ angles between 15° and 165° are held against the surface of the cryostat by a structure made from folded sheet aluminum which was attached using aluminum studs spot welded to the cryostat. The scintillator in the lower part of the detector rests on the bottom of the cryostat and is self-supporting on the sides. This results in significant deviations from a nominal geometry of equally spaced bars in ϕ, but a photographic survey of the bar positions was carried out after installation to determine their locations. Since then their surveyed positions have been refined by analyzing collision data and the ϕ angles of the bar centers are currently understood to better than 2 mrad.

A Hamamatsu R7761 nineteen-stage fine-mesh photomultiplier tube (PMT) with a diameter of 1.5 inches, is attached to each end of every bar. These can operate in the 1.4 Tesla magnetic field of the CDF solenoid with an average gain reduction factor of 500 from the nominal gain of 10^6. The optical connection between the PMT and the scintillator is made using a compound parabolic concentrator (CPC), attached to the PMT using optical cement. A good interface between the CPC and the scintillator is achieved using a silicone optical coupling pad that is compressed between them using the force applied by a spring. The voltage divider base is constructed using surface mount components on a printed circuit board, soldered directly to the leads of the PMT. A preamplifier is attached via a connector on the base. A small printed circuit board serves as a light seal and brings high voltage for the base and low voltage for the preamplifier into the assembly and signals from the preamplifier out. This entire assembly is mounted inside a 1.5 inch diameter hole bored in an aluminum block with approximately the same transverse dimensions as the scintillator. A spring forces the assembly against the scintillator, insuring a good connection at the silicone optical coupling pad interface.

B. The Front End Electronics

Figure 2 shows the signal path for a single PMT channel. The preamplifier receives a nearly differential input

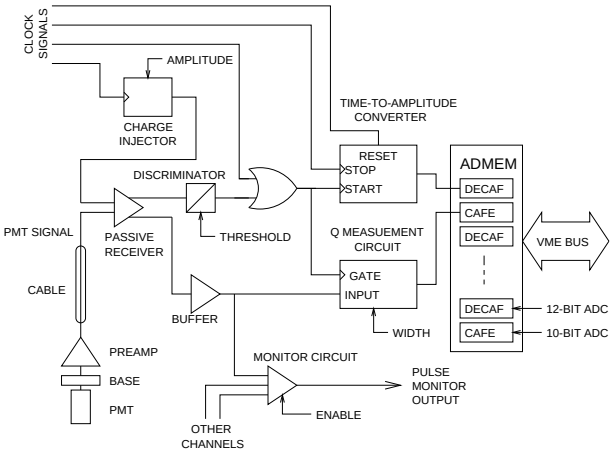

Fig. 2. A block diagram of the electronics processing chain for the signal from one PMT channel. Most of the signals are indicated by single lines for clarity but are actually differential signals.

formed from the anode and last dynode stage of the PMT. Its differential output is transmitted on shielded twisted pair cable a distance of approximately 12 meters to the front-end electronics that resides in a VME crate mounted outside the detector. The received signal is split between two signal paths: one for the timing measurement and the other for a measurement related to the pulse height.

The timing path enters a discriminator with an adjustable threshold. The discriminator output provides a start signal to a Time-to-Amplitude Converter (TAC). The TAC ramp is terminated by a common stop clock edge. The voltage output from the TAC is sampled by a 12-bit ADC whose data is buffered by a VME module, referred to as the ADMEM[4], which was designed originally to read out PMT signals from CDF's calorimeter systems. The least count of this TDC corresponds roughly 17 ps and the available dynamic range is typically 60 ns.

The common stop signal has its phase correctly adjusted with respect to the time at which the p and $\overline{p}$ collide and is fanned out to all electronics channels in the system. This is implemented using a dedicated set of modules that first distributes differential ECL clock signals to each of 8 crates of electronics, and then to six TOF electronics modules within each crate. This same system generates a reset signal for the TAC and distributes it, along with a clock signal used for calibration, to all electronics channels.

The primary purpose for measuring the charge of the PMT signals is to perform a correction for the discriminator walk, or time slewing, due to pulses of varying amplitude. The charge measurement path converts the received voltage signal from the preamplifier into a current that is passed to a charge sensitive ADC located on the ADMEM module. The current driver circuit is switched by a gate of adjustable width, initiated by the discriminator output, so that only the charge due to the pulse that fired the discriminator is integrated.

In addition to these basic operations, the front-end electronics provides several services necessary for configuration, monitoring, calibration and testing. An FPGA interfaces with one VME register and is used to set all discriminator thresholds and gate widths and to provide control over the state of the calibration and monitoring circuits. Various clock signals can be output via a BNC connector to be monitored at a remote location. This capability proved to be very useful during the initial installation and commissioning. A second BNC output is driven by a current summing circuit to monitor the PMT pulses from selected channels.

Calibration of the electronics is performed using a digital delay generator (DDG) to initiate a differential ECL pulse that is fanned out to selected sets of channels. This signal is used to start the TAC, bypassing the discriminator. By stepping through a series of delays with respect to the common stop signal, the response of the TAC to known delays can be measured. A second mode of calibration uses the same pulse to trigger a circuit that injects a signal resembling a PMT pulse into the receiver circuit. This was primarily used for built-in self-tests of the electronics prior to installation.

IV. Performance and Test Results

The installation of the front-end electronics was completed in August, 2001 and has been studied in a variety of ways. The stability of the electronics has been studied using the calibration circuits described in section III-B and we have begun to study the performance of the complete system using $p\overline{p}$ collision data recorded in August, September and October of 2001.

A. Electronics stability

The stability of the entire electronics chain was initially studied by generating the common stop signal delayed with respect to a calibration pulse using a fixed length of cable. The resulting TDC distributions had typical RMS widths of 8.5 ps and their mean values were found to be stable at the level of 9 ps over the 40 hour duration of the study. Similarly, using the DDG to generate the delay between the calibration pulse and the common stop resulted in typical RMS widths of 25 ps, but this includes an additional component due to the jitter of the DDG.

The response of the TDC to a sequence of known delays has been studied using the DDG with the generated time interval measured using a digital oscilloscope. We have found the response to be not completely linear but parameterize the nonlinear effects by a function of the form

$$V_{\rm TAC} = \beta(1 + \gamma e^{-t/\tau})t \qquad (2)$$

where β, γ and τ are parameters determined from a fit to the set of generated delays. The deviation of the measurements from the fitted curve are Gaussian distributed with a width of 5.1 ps. This parameterization adequately describes the response of all 432 channels in the system.

B. Time difference measurements

The time at which a PMT pulse is registered, measured with respect to the nominal $p\overline{p}$ bunch crossing time, can be modeled by the formula

$$t = c + t_0 + tof + (L/2 \pm z)/s - \alpha \log(Q/Q_0) \qquad (3)$$

where c is a constant term, t_0 represents the time at which the $p\overline{p}$ interaction occurred, tof is the time-of-flight of the particle impinging on the bar of scintillator of length L, s is the effective speed of light propagation in the scintillator and the logarithmic term is an empirical parameterization for the time slewing correction. The z coordinate is measured along the length of the bar and is positive on the east end of the detector. The positive and negative sign of the term proportional to z corresponds to the case where a PMT is on the west or east end of the detector, respectively. Since the TAC is read out using a common stop configuration, small TDC values correspond to large times measured with respect to the beam crossing time.

When a single track enters a bar of scintillator, the difference in the times read out on east and west ends is essentially a linear function of z, the track's entrance point along the bar. A typical distribution of the time difference plotted as a function of z is shown in Fig. 3

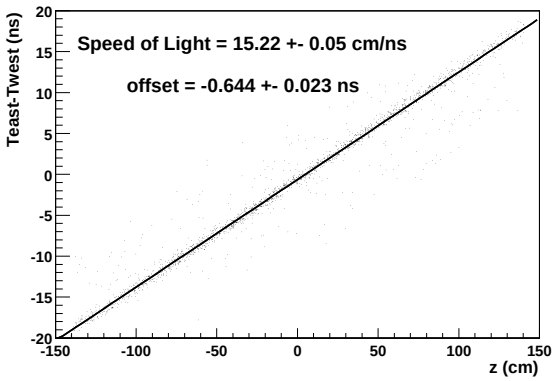

Fig. 3. Distribution of the time difference, $t_{\rm east} - t_{\rm west}$, plotted versus the entrance point, z, of a track. The scattered points away from the fitted line are due to multiple tracks hitting the bar.

We observe a range of values for the effective speed of light for each bar, s, which has a mean value of about 15 cm/ns. The exact values measured depend on operating conditions such as discriminator thresholds and PMT gains and can depend on the attenuation length of light in the scintillator due to the time slewing effect. The width of the residuals from this straight line fit are then a measure of the timing resolution of each PMT, added in quadrature. This analysis was applied to all bars in the system and the average resolution of $t_{\rm east} - t_{\rm west}$ is plotted as a function of z in Fig. 4. The resolution averaged over all bars in the system is typically 250 ps or better. Since this measures the resolution of two channels added in quadrature, it differs by approximately a factor of two from the resolution expected for a calculation of the mean time from

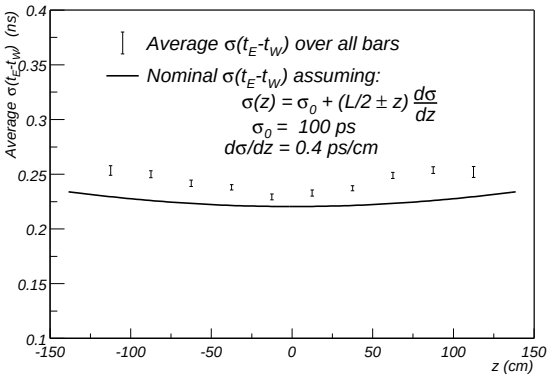

Fig. 4. Average width of the $t_{\rm east} - t_{\rm west}$ residual for all bars, as a function a track's entrance point along the bar.

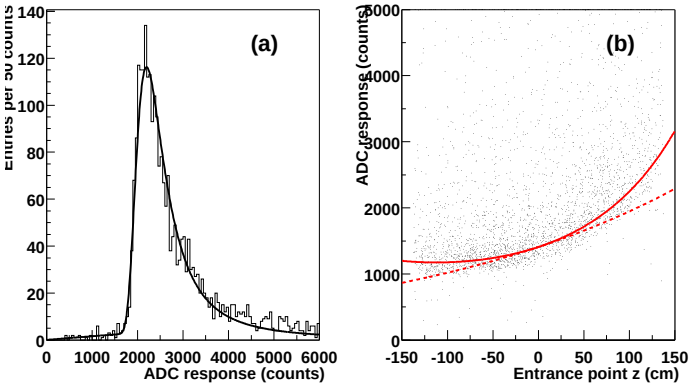

Fig. 5. (a) The ADC response, corrected for attenuation length effects, fit to a Landau function. (b) The distribution of ADC response as a function of z. The dotted curve is a pure exponential attenuation model, while the solid curve includes a z^2 term in the exponent.

which the time-of-flight is calculated. The measured time difference resolution can be compared to the parameterization of the timing resolution that was used for design studies [3]. This comparison is also shown in Fig. 4 and indicates that the timing resolution, evaluated in this way, is close to our design goals. However, as systematic effects can cancel in the time difference measurement, but would not necessarily cancel in the calculation of time-of-flight, this estimate of the timing resolution only represents the intrinsic capabilities of the detector.

C. ADC response

The response of the ADC has been studied using a sample of tracks which are isolated to a single bar and thus have a well understood path length in the scintillator. Tracks which enter the scintillator in a narrow region in z are found to have an ADC response that is well described by a Landau distribution. The variation in the peak position as a function of z has been found to deviate from that of a pure exponential which would normally be attributed to the attenuation of light in the scintillator. Instead, an additional factor with an exponential term proportional to z^2 is needed to accurately describe the ADC response as a function of z which we hypothesize is due to reflection of light of the ends of the bars. These effects are shown for a typical PMT in Fig. 5, in which the distribution of the ADC response as a function of z is plotted along with the ADC response, corrected for the attenuation effects and fitted with a Landau distribution. These data were recorded with the PMT operated at a nominal gain of 5×10^4 and with the width of the charge measurement gate set to approximately 17 ns. The width of the Landau peak divided by the peak position is typically 8-10% for all channels. The attenuation length measured for all the bars in the system ranges from 200 to 450 cm with a mean value of 330 cm.

D. Time slewing correction

We have studied the effects of pulse height on the measured time using a sample of tracks that pass through adjacent bars of scintillator. Depending on the path length in each bar, a range of ADC responses can be obtained in the two channels at the same ends of the bars. Because the z-coordinate of the track's entrance point in each bar is similar, the time difference between the two channels would be nearly identical except for time slewing effects.

As shown in equation 3, the correction to the measured time has been parametrized by a logarithmic function of the ADC response where the parameter α is determined separately for each channel in the system. For a restricted range in z, the width of the distribution of time differences on adjacent channels provides an indication of the timing resolution obtained after the time slewing correction. This is found to be an almost linear function of z and is plotted in Fig. 6. The results from this analysis are similar

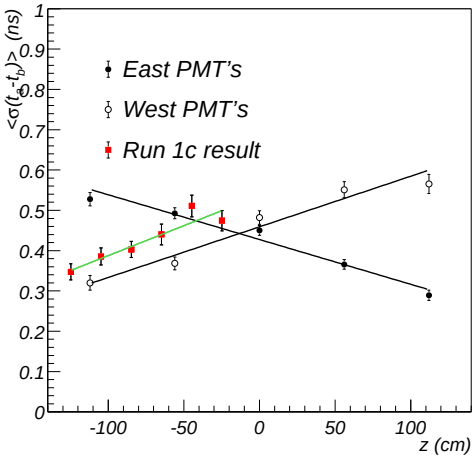

Fig. 6. Average width of the time difference distribution, corrected for time slewing, measured on adjacent PMT channels, as a function of a track's entrance point in z.

to those obtained from the 20 bar Time-of-Flight test sys-

tem [5]. The resolution is expected to be worse than the values obtained from the east-west time difference resolution because the light is divided between the two bars and because of systematic effects that do not cancel in this time difference measurement.

E. Preliminary Particle Identification Performance

After applying the corrections described in the previous sections, the constant time offset of each channel can be determined. This allows the time difference between two tracks in any two bars in the system to be measured with sufficient precision to begin an initial study of particle identification. Using data collected in Fall 2001, peaks in the TOF mass distribution from pions, kaons, protons and deuterons have been seen. Currently, the resolution is dominated by the uncertainty in the calibration constants determined for each channel and improvements are expected from a variety of sources. First, the presence of several tracks in the event that can be used to define the collision time will reduce the uncertainty on measured time-of-flight. For triggered events containing the decay $B^0 \to J/\psi K^0_S$, one expects typically 10 tracks to be available to define the collision time and the uncertainty on this time is expected to be reduced to approximately 30 ps. Even so, the resolution currently obtained is expected to be adequate to provide an unbiased calculation of the collision time. This will allow the times recorded on individual channels to be studied in more detail and will provide a second, more refined, set of calibration parameters.

V. Conclusion

The installation of all hardware associated with the CDF-II Time-of-Flight detector has been completed and we are currently in the process of commissioning the system. The results obtained so far indicate that the ultimate timing resolution should meet the specifications on which our physics studies have been based. We have only begun the process of using the completed detector system for particle identification and are still developing the algorithms necessary to fully exploit the capabilities of the electronics.

References

[1] R. Blair et al., "The CDF-II Detector: Technical Design Report," FERMILAB-PUB-96-390-E.

[2] C. Paus et al., "Design and Performance Tests of the CDF Time-of-Flight System," *Nucl. Instrum. Meth.*, vol. A461, pp. 579–581, 2001.

[3] C. Grozis et al., "The Time of Flight Detector at CDF," *Nucl. Phys. Proc. Suppl.*, vol. 93, pp. 344–347, 2001.

[4] Theresa Shaw, Charles Nelson, and Thomas Wesson, "The Design of the CDF Run 2 Calorimetry Readout Module," *IEEE Trans. Nucl. Sci.*, vol. 47, pp. 1834–1838, 2000.

[5] F. Ukegawa et al., "Results from a 20 scintillator bar time-of-flight test system located inside the 1.4-T CDF solenoid," *Nucl. Instrum. Meth.*, vol. A439, pp. 65–79, 2000.